AD-A096 228 ILLINOIS INST OF TECH CHICAGO DEPT OF METALLURGICAL --ETC F/G 11/6
THE MECHANISMS OF CRACK INITIATION AND CRACK PROPAGATION IN MET--ETC(U)
DEC 80 P GORDON N00014-79-C-0580

UNCLASSIFIED NL

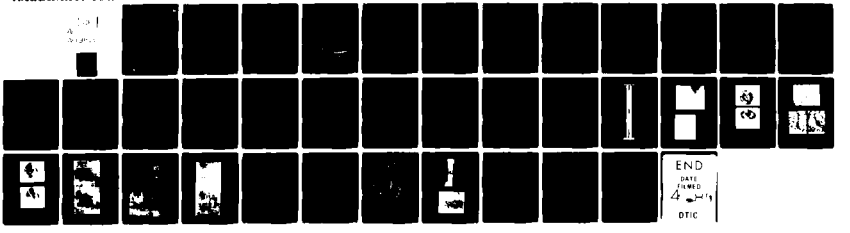

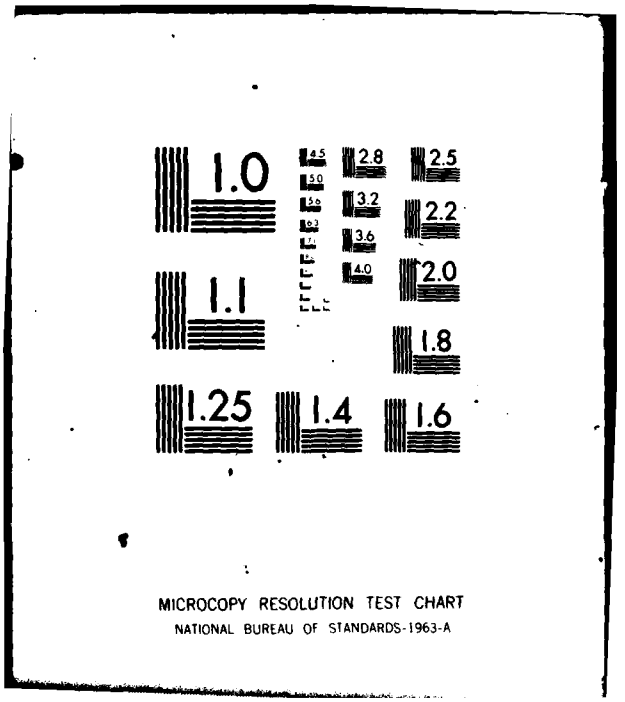
1.0
1.1
1.25
1.4
1.6
1.8
2.0
2.2
2.5
2.8
3.2
3.6
4.0
4.5
5.0
5.6
6.3
MICROCOPY RESOLUTION TEST CHART
NATIONAL BUREAU OF STANDARDS-1963-A

THE MECHANISMS OF CRACK INITIATION AND CRACK PROPAGATION IN METAL-INDUCED EMBRITTLEMENT OF METALS

PART I. DELAYED FAILURE IN THE EMBRITTLEMENT OF 4140 STEEL BY INDIUM

TECHNICAL REPORT 12-12-80

Submitted by

Paul Gordon
Dept. of Metallurgical and Materials Engineering
Illinois Institute of Technology
Chicago, Illinois

To

The Office of Naval Research
Contract No. N00014-79-C0580

December 12, 1980

(9) Technical rept. 1 Jun 79-31 Dec 80.

SECURITY CLASSIFICATION OF THIS PAGE (When Data Entered)

REPORT DOCUMENTATION PAGE	READ INSTRUCTIONS BEFORE COMPLETING FORM
1. REPORT NUMBER: 12-12-80	2. GOVT ACCESSION NO.: AD-A096 228	3. RECIPIENT'S CATALOG NUMBER
(6) 4. TITLE (and Subtitle): THE MECHANISMS OF CRACK INITIATION AND CRACK PROPAGATION IN METAL-INDUCED EMBRITTLEMENT OF METALS. Part I. Delayed Failure in the Embrittlement of 4140 Steel by Indium	5. TYPE OF REPORT & PERIOD COVERED: Technical Report 6/1/79 to 12/31/80
	6. PERFORMING ORG. REPORT NUMBER
7. AUTHOR(s): (10) Paul Gordon	8. CONTRACT OR GRANT NUMBER(s): (15) N00014-79-C0580, NSF-DMR 79-01674
9. PERFORMING ORGANIZATION NAME AND ADDRESS: Metallurgical and Materials Engineering Dept. Illinois Institute of Technology 3300 S. Federal St., Chicago, Illinois 60616	10. PROGRAM ELEMENT, PROJECT, TASK AREA & WORK UNIT NUMBERS: (11) 12 Dec 80
11. CONTROLLING OFFICE NAME AND ADDRESS: Office of Naval Research Department of the Navy 800 N. Quincy St., Arlington, Virginia 22217	12. REPORT DATE: 12-12-80
	13. NUMBER OF PAGES: 18 + 15 figures (12) 37
14. MONITORING AGENCY NAME & ADDRESS (if different from Controlling Office): Dept. of the Navy, Office of Naval Research Branch Office Chicago, 536 S. Clark Street, Chicago, IL 60605	15. SECURITY CLASS. (of this report)
	15a. DECLASSIFICATION/DOWNGRADING SCHEDULE
16. DISTRIBUTION STATEMENT (of this Report): [illegible]	
17. DISTRIBUTION STATEMENT (of the abstract entered in Block 20, if different from Report)	
18. SUPPLEMENTARY NOTES	
19. KEY WORDS (Continue on reverse side if necessary and identify by block number)	

20. ABSTRACT (Continue on reverse side if necessary and identify by block number)

Metal-induced embrittlement (MIE) of 4140 steel by indium has been studied using delayed failure tensile tests. The temperature and stress dependence of the kinetics of crack initiation and crack propagation in both liquid metal-induced and solid metal-induced cracking have been examined in the same system for the first time in MIE. This was done using electrical potential-drop measurements along the indium-covered portion of the sample gage length to record the start and progress of cracking, and also through fractographic observations. In Part I of the report on this work, the

DD FORM 1 JAN 73 1473 EDITION OF 1 NOV 65 IS OBSOLETE
S/N 0102-LF-014-6601

SECURITY CLASSIFICATION OF THIS PAGE (When Data Entered)

400 234

experimental results are presented and their implications with regard to crack propagation are discussed. In Part II, various mechanisms proposed in the literature for crack initiation are evaluated in the light of the experimental results and other known characteristics of MIE, and a new mechanism is proposed which, it is believed, synthesizes and rationalizes the available evidence best.

THE MECHANISMS OF CRACK INITIATION AND CRACK PROPAGATION IN METAL-INDUCED EMBRITTLEMENT OF METALS. PART I

ABSTRACT

Metal-induced embrittlement (MIE) of 4140 steel by indium has been studied using delayed failure tensile tests. The temperature and stress dependence of the kinetics of crack initiation and crack propagation in both liquid metal-induced and solid metal-induced cracking have been examined in the same system for the first time in MIE. This was done using electrical potential-drop measurements along the indium-covered portion of the sample gage length to record the start and progress of cracking, and also through fractographic observations. In Part I of the report on this work, the experimental results are presented and their implications with regard to crack propagation are discussed. In Part II, various mechanisms proposed in the literature for crack initiation are evaluated in the light of the experimental results and other known characteristics of MIE, and a new mechanism is proposed which, it is believed, synthesizes and rationalizes the available evidence best.

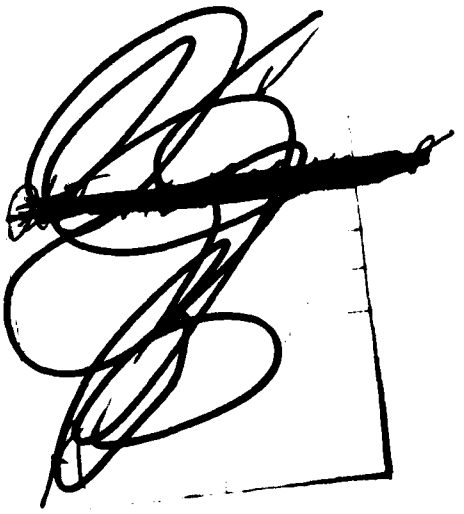

THE MECHANISMS OF CRACK INITIATION AND CRACK PROPAGATION IN METAL-INDUCED EMBRITTLEMENT OF METALS
PART I. DELAYED FAILURE IN THE EMBRITTLEMENT OF 4140 STEEL BY INDIUM*

Paul Gordon[+] and Henry An[‡]

INTRODUCTION

When normally ductile solid metals are placed under tensile stress and simultaneously into intimate contact with certain lower-melting metals, they tend to fracture at abnormally low stresses. Since the lowered fracture stress can be below the normal yield stress and since the effect has been most commonly noted when the low-melting metal actually was in the liquid state, the phenomenon was labeled liquid-metal embrittlement (LME). It is now clear, however, that the embrittler can produce a similar effect when in the solid state, (c.f., (1)); the phenomenon is, thus, more appropriately called metal-induced embrittlement (MIE) or, as the case may be, liquid metal-induced embrittlement (LMIE) or solid metal-induced embrittlement (SMIE).

There have been several different theories proposed to account for MIE (actually for LMIE) on an atomic level. These include the bond-breaking model of Stoloff and Johnston (2) and Westwood and Kamdar (3) in which it is proposed that the adsorption of the embrittler atoms at the tip of a crack in the base metal lowers the cohesive bond energy of the base metal surface atoms sufficiently to make tensile decohesion at the crack tip easier than crack blunting by dislocation flow when stress is applied, leading to brittle fracture; the stress-assisted dissolution model of Robertson (4), later also proposed by Glikman, et al. (5), in which it is hypothesized that a crack propagates because the highly stressed atoms at its leading edge are dissolved into, and carried away by diffusion through, the liquid embrittler; the embrittler penetration model of Krishtal (6), in which it is supposed that cracking takes place because the lowering of surface energy produces dislocations which pile

---

*Based on the Ph.D. thesis research of Henry An, in the Dept. of Metallurgical and Materials Engineering, Illinois Institute of Technology

[+]Professor, Dept. of Metallurgical and Materials Engineering, Illinois Institute of Technology

[‡]Ph.D. candidate, Dept. of Metallurgical and Materials Engineering, Illinois Institute of Technology

up against grain boundaries embrittled by diffusion-penetration of the embrittler atoms into the base metal ahead of the advancing crack to distances of the order of tens of atomic diameters; and the surface-structure model of Lynch (7) in which it is proposed that the role of the embrittler atoms adsorbed at the crack tip is to so alter the atomic structure of the base metal surface atoms as to considerably lower the normally high stress necessary to generate and move dislocations at the tip, thus lowering the stress for fracture by slip.

None of these models has received universal acceptance, though the bond-breaking model has been most generally accepted because it seems to account for more of the experimental observations than the others. Two papers are presented here as a report on the first phase of an effort to help identify the correct MIE model by taking advantage of a little-studied feature of MIE, namely, delayed failure. If a metal in contact with an embrittler is placed under a fixed tensile load of a magnitude less than that necessary to fracture it at once, it will, in most cases, undergo a form of static fatigue – delayed failure – in which fracture takes place at constant load after a substantial length of time – up to several hours, or even longer depending on the load and the temperature. For a given embrittlement couple (the base metal-embrittler combination), we have found that the time to failure is both stress and temperature dependent. The phenomenon thus presents a clear opportunity to study the kinetics of the cracking process and consequently to obtain significant information on the underlying mechanisms. Until the present work, however, only a few delayed failure studies have been carried out (8 through 16) and of these only three published works (8,10,11) used techniques capable of distinguishing the initiation from the propagation of the embrittlement crack. In addition, the temperature and stress dependencies have not been thoroughly studied.

In the present work, pure indium (melting point 156°C) has been used as the embrittler applied to smooth (unnotched) tensile samples of commercial 4140 steel quenched and tempered to a room temperature ultimate tensile strength of 1500 $\pm$ 12 MPa (218 $\pm$ 2 ksi). The samples were tested under various fixed initial stresses ranging from about the proportional limit to just above the 0.2% offset yield strength at temperatures in the range 107 to 182°C. Thus, for the first time in SMIE, the same embrittlement system has been studied extensively both in the SMIE and the LMIE range. In each test, the electrical potential drop produced by a constant current

over that portion of the sample gage length covered by indium was monitored. When a crack formed, the otherwise constant potential drop increased and continued to do so during crack propagation; the data thus provided a measurement of both the crack initiation time and the crack propagation time as a function of test temperature and initial stress, again for the first time in MIE studies.

In this first paper the experimental results of the delayed failure tests are given and their implications with respect to crack propagation discussed. In a second paper, which follows directly, theoretical considerations on crack initiation and a proposed new mechanism of MIE are presented.

EXPERIMENTAL DETAILS

The indium used in this investigation was reported by the supplier (Indium Corp. of America) to be 99.999% pure. The steel was obtained in the form of 5/8" round bars of commercial 4140 steel, all from the same heat, having the composition indicated in Table 1. Cylindrical delayed failure tensile samples were rough-machined from these bars, heat treated, and then final-machined to a gage length of 42 mm and a gage diameter of 5.84 mm. The gage surface was given a mechanical polish to 600 grit followed by electropolishing. The final gage diameter was just under 5.84 mm, measured to within 0.1%.

Table 1. Chemical Composition of 4140 Steel Samples

	Weight Percent	
Element	Heat Analysis	Bar Analysis
C	.41	.39
Mn	.87	.86
P	.014	.01
S	.016	.03
Si	.23	.25
Ni		.11
Cr	.96	.92
Mo	.18	.15
Cu		.1

Preliminary work indicated that the most convenient delayed failure test temperatures and times would be obtained with samples having a tensile strength of 1500 MPa (218 ksi); thus, all samples were heat treated to produce this strength. Only two samples were actually tensile tested (continuous loading) to failure at room temperature; the strength of the others was checked by hardness measurements and all were found to be R_c 45.5 ± .3, which is equivalent to a tensile strength of 1500 ± 12 MPa (218 ± 2 ksi). This close control of the strength was obtained by carefully regulating all heat treatment conditions. Austenitizing was done in air in a muffle furnace containing a heavy steel cylinder to smooth out temperature

variations. The austenitizing treatment was 60 minutes in the pre-heated furnace followed by oil quenching. During the final 20 minutes the sample was at 846° ± 1°C (1555 ± 2°F). Tempering was carried out in a lead bath for 60 minutes at 427 ± 1/2°C (800 ± 1°F). The average fracture grain size of the heat treated samples was about 0.01 mm (c.f., later Figure 4).

The preliminary testing (and previous work, e.g. (16)) revealed that the most serious source of scatter in the results was improper application of the embrittler. We have found that the main requirements of proper application are: (a) thorough "wetting" – if this was not accomplished, cracking tended to be very late, and, in SMIE, many small "thumbnail" cracks formed around the periphery of the sample surface; with good wetting, on the other hand, there was always only a single crack, in both SMIE and LMIE, which in SMIE formed a ring of almost uniform depth all around the sample periphery (see later, Figure 3); (b) the good flow that comes with good wetting had to be confined to an annular band of uniform thickness and length (along the gage length) – free flow formed regions of very thin indium coverage in which cracks appeared to initiate prematurely but then stopped propagating into the steel when the crack broke through the indium to the atmosphere (presumably because of oxidation of the crack surface). The technique finally devised to produce these requirements consisted of the following steps: (1) application of a heat resistant silicone-phenolic resin to the gage length leaving uncovered only a 4 mm wide band at the center of the gage length; (2) initial application of the indium to this band by electroplating; (3) melting of the electroplated indium under a soldering flux by torch-heating while spinning the sample on a lathe; (4) removal of the resin, cleaning, and filing of the indium band to a final thickness of .25 mm. A typical prepared sample is shown in Figure 1. The flux used in the melting of the indium was a commercial soft-solder flux containing zinc chloride, tin chloride, and ammonium chloride. Previous embrittlement testing (15) had shown that the flux did not in itself produce embrittlement. We also carried out standard hydrogen embrittlement tests at room temperature on indium-plated samples to show that no effect of this kind was introduced by our plating procedure.

Delayed failure tensile testing was carried out on a dead-load Satec stress-rupture machine provided with a temperature-controlled furnace (air atmosphere)

and universal type specimen gripping devices to minimize bending. During testing the temperature of the sample was measured with a chromel-alumel thermocouple spot welded to the sample surface next to the indium band. The temperature was continuously recorded and held constant to better than $\pm$ 1/2°C. The uncertainty in the indicated initial stress levels was $\pm$ 3 MPa, due largely to the error associated with sample diameter measurement.

Crack initiation and propagation were monitored by passing a 15-ampere electric current along the sample and measuring the potential drop along a 5 - 6 mm gage length of the sample centered on the indium band. The current was controlled by an NJE Corp. power supply, both current and voltage regulated to .01% of load. The usual total potential drop was 1.8 - 2.0 mv, which was continuously recorded. The smallest detectable potential change was 0.001-0.002 mv, whereas the total potential change during the brittle crack development was approximately .1 mv.

RESULTS AND DISCUSSION

General Characteristics of the Fractures

Fracture in our delayed failure tensile tests was found to take place in three stages. The first stage consisted of an incubation, or initiation, period during which there was no detectable crack, both in SMIE and in LMIE. The presence of this incubation period was noted for all samples, primarily by the initial constancy in the electrical potential drop vs. time curves obtained (see Figures 6-8). It was recognized, however, that the sensitivity of the electrical measurements to very small cracks was not high – it is estimated that a crack of cross-sectional area about 0.15 mm^2 (say, 1.5 mm long by .1 mm deep) would be the smallest detectable by these measurements. To discover whether much smaller cracks were present during the incubation period, for both SMIE and LMIE several interrupted delayed failure tests were run in which the samples were held under load for up to 90% or more of the expected incubation time, the load released and the indium removed*. The samples were then deep-acid etched (50% HCl-H_2O at 70°C for 1/2 hour) and the surfaces examined in the scanning electron microscope (SEM) for cracks. None was observed; a representative sample surface is shown in Figure 2. An estimate of the size of crack which could easily have been observed had it been present can be obtained by noting that the inclusions in the steel can readily be observed in Figure 2 as small, longitudinal elongated etch pits. The smallest of these which we could readily identify were about .02 x .002 mm in size; since MIE cracks would be transverse to the inclusions and the etch exaggerates their size, we could undoubtedly have detected the presence of cracks considerably smaller than this had they existed, say, .01 mm long by .001 mm deep. Thus, if we designate as t_i the time at which the potential drop curve first is detected to change, then we conclude that any crack present prior to t_i could have been at .9 t_i no larger than about $10^{-5}/.15$, or about 10^{-4} times the size of the crack at t_i. This point will be discussed further later.

*Indium was removed by reheating and brushing the molten indium off.

In the literature only three publications and two unpublished works bear on the question of an incubation period for crack initiation in MIE. Rostoker, et al. (8) concluded from LMIE delayed failure tensile tests that (a) in an incubation period in which the tensile properties did not change, no cracks were present, and (b) the incubation period consumed most of the time to failure. Nichols and Rostoker (10) showed one dilatometer curve in which, during an 18-minute delayed failure test in LMIE, changes in specimen length occurred only during the last minute. They also carried out interrupted delayed failure tests and found no cracks on the sample surface before final failure. Zych (14), in high strain-rate LMIE tensile tests with total failure times between 10^{-3} and 10^{3} seconds, found initiation times were always a large fraction of the failure times. These findings agree with ours. On the other hand, Iwata, et al. (11) present one length-change curve and Lynn (15) in unpublished work carried out one interrupted-delayed failure series, both in SMIE, in which crack propagation was reported to have started immediately on loading. Kassner (16), also in unpublished work, using delayed failure tensile tests found a substantial incubation period in LMIE but not in SMIE. We believe the latter SMIE result was due to experimental difficulties. All of the other apparently inconsistent results from different investigators can be rationalized on the basis of a new mechanism for MIE proposed in Part II of this report on our present work.

The second stage of delayed failure is the embrittler-dependent propagation of the initiated crack. It has long been established (e.g., (17)) that the crack propagates during this stage only so long as embrittler is available at the crack tip. A detailed discussion of the nature of the possible embrittler transport processes and predictions of the probable operative ones have been given by Gordon (18); one purpose of the present work is to check these predictions. The macroscopic appearance of this stage of the fracture is illustrated in the fractographs of Figure (3) through (5) for SMIE and LMIE. In SMIE (Figure 3), the embrittler-dependent crack forms a ring at the periphery of the fracture surface. In every case this ring was found to be about .6-.8 mm deep at its greatest depth and, on the opposite side of the periphery, the crack usually showed a radial ledge or step. This is interpreted to mean the nucleation event took place on the cylindrical surface at the point of greatest crack depth, that the crack then grew circumferentially in both directions,

meeting at the ledge, and at the same time grew radially, with the rate in this direction being the propagation bottleneck and being determined by the rate at which the embrittler could be transported to the advancing crack tip. (With good wetting, indium is always immediately available at the sample surface, so that the rate of circumferential propagation near the sample surface is always much greater than that radially.) No indium could be seen on the crack surface and none could be detected by the x-ray energy dispersive capability of the SEM; there is no doubt, however, from the literature, from theoretical considerations, and from the appearance of the crack surface itself that the indium is there in a thin layer, as discussed later. The thickness of the layer is below the detectability of the SEM-EDX. The intergranular nature of the apparently brittle portion of the fracture is illustrated in Figure 4a.

In LMIE the embrittler-dependent portion of the crack tends to be less regular in shape, appears on only one side of the fracture surface, and is covered with a layer of indium thick enough to be seen readily by eye (Figure 5). This appearance is due to the very rapid rate of embrittler transport radially as discussed later. It has been shown many times in the literature that such LMIE fractures in polycrystalline steel are also intergranular.

The third stage of the failure process is reached in both SMIE and LMIE when the stress intensity at the crack tip has exceeded the critical stress intensity for normal ductile failure. The crack then propagates independently of the embrittler – essentially "runs away" from the embrittler – producing the final catastrophic failure; the central region of the fracture surface in SMIE (Figure 3) and that portion not covered by indium in LMIE (Figure 5) correspond to this final stage of fracture. Figures 4b and c illustrate the dimpled rupture characteristics of this fracture stage.

Typical Delayed Failure Potential-Drop Curves

Figure 6 presents a typical potential drop-time curve for a delayed failure test in LMIE. It is clear that no detectable potential change takes place for an extended time period after loading – in this case, 511 seconds – and then the potential drop increases precipitously as fracture takes place in a time shorter than the lower limit of our experimental sensitivity. The crack propagation – both embrittler-dependent

and embrittler-independent stages – takes place during the period of less-than-1 second of precipitous potential rise (later experiments narrowed this to 0.1 second). The embrittler transport rate along the fracture surface must be extremely high, confirming the deduction that the transport can only be by bulk liquid embrittler flow, as discussed by Gordon (18).

Typical potential drop-time curves for delayed failure tests in SMIE are shown in Figures 7 and 8. Here, again, there is an incubation period – for 4.50×10^4s (12.5 h) in Figure 7 and 4.07×10^3s (1.13 h) in Figure 8. Then the potential drop rises and continues to do so at an increasing rate for $.43 \times 10^4$s (1.2 h) in Figure 7 and $.24 \times 10^4$s (.67 h) in Figure 8. This is the embrittler transport-controlled stage of the crack propagation. There is, alternatively, some possibility that in this stage, the propagation is discontinuous, as in hydrogen embrittlement cracking, and that, therefore, the propagation rate is determined by crack re-initiation rather than embrittler transport. Our curves, however, do not exhibit discontinuous propagation – we have been able to show that any apparent propagation discontinuities which appear are in fact inherent in our recorder. This was done by noting the curve characteristics during temperature increase before testing and temperature decrease after failure. In every case, any jogs noticed during the crack propagation stage were duplicated in size and shape during the heat-up or cool down period when the only change taking place was the smooth change in temperature. We, therefore, conclude that any crack re-initiation taking place during the crack propagation (such as at grain boundaries) was unimportant compared to actual crack movement itself. Again, as in LMIE, we define the initiation time as that time at which the shape and magnitude of the potential drop curves begin to change detectably. The end of the embrittler-dependent propagation period is indicated by the final precipitous rise in potential drop which accompanies the much faster final ductile fracture stage.

Crack Propagation and Embrittler Transport

Figure 6 demonstrates that in LMIE once the crack gets underway, both the embrittler-controlled, and the ductile, portions of the crack formation are over in less than about one second. (This was narrowed to .1 second in other tests.) This was found to be true at all temperatures and at all loads (for which failure took place) in our LMIE tests (13 tests in the temperature range of 158° to 183°C and initial stresses from 1068 to 1226 MPa (155 to 178 ksi). As shown by Gordon (18) the only feasible embrittler transport mechanism consistent with such a high propagation rate in indium is bulk liquid flow*.

In SMIE the embrittler-controlled crack propagation rate is much lower, as shown in Figures 7 and 8. The curves in Figures 7 and 8 are typical of all our SMIE tests-to-failure — some 26 tests in the temperature range 114° to 154°C and the initial stress range 1068 to 1226 MPa (155 to 178 ksi). The propagation times from initiation to catastrophic failure at various stress levels are plotted in Figure 9 as a function of temperature and in Figure 10 as a function of stress. Though there is a substantial scatter in the data, certain trends are clear:

(a) *There is a large, discontinous increase in propagation time at the indium* melting point from times of less than 0.1 second in LMIE to times in the range 500-2000 seconds in SMIE. Thus, the transport mechanism in SMIE is clearly different and much slower than that in LMIE. Since bulk liquid flow and vapor phase transport are not possible here (for the latter the vapor pressure of indium is much too low — see (18)), some diffusion mechanism must be responsible. An approximate experimental diffusion coefficient can be obtained from the transport times by using the expression (see for example (20))

$$D \cong \frac{X^2}{2t} \qquad (1)$$

and the known crack depth of about .7 mm. At 156° in SMIE, this gives $D \cong 2 \times 10^{-4}$ mm^2/sec. Of the various conceivable diffusion mechanisms — volume

*The actual transport time, according to Gordon (18), is of the order of 10^{-3} seconds. Experimental measurements of crack paopagation rates in LMIE (for example (12), (14), (17) and (19)) indicate the time for transport in our LMIE tests would be in the range .03 to .003 seconds.

or grain boundary diffusion of indium through the steel, first monolayer surface diffusion of indium over the steel crack surface, or surface self-diffusion of indium over indium already deposited on the steel crack surface by a "waterfall" mechanism, all but the last are expected to be too slow by many orders of magnitude at these temperatures (see (18)). Following the ideas of Gjostein (21), the surface self-diffusion coefficient of solid indium at its melting point can be expected to have a value of the order 10^{-1} to 10^{-3} mm^2/sec. This is within reasonable range of our experimental value of 2×10^{-4}. The factor of approximately 50 discrepancy can be accounted for in one or more of the following ways: (i) Since it is postulated that the indium transport proceeds by indium atom diffusion over a number of indium atom layers which themselves are layed down at the advancing edge of the indium by a "waterfall" effect, then the appropriate time to be used in equation (1) is not the total propagation time but rather this divided by the number of indium atom layers. Thus, if there were 50 atom layers of indium, the discrepancy would disappear – and such a coating of indium on the crack surface would still not be visible to the unaided eye or detectable by SEM-EDX. (It would, however, be detectable by Auger measurements; such experiments would be very useful on this point); (ii) If there are only one or two atom layers of indium, the diffusing atoms might "feel" the slowing effect of the relatively stationary iron atoms below; (iii) oxygen or other gas atoms may be slowing the indium diffusion – our experiments are carried out in air and we depend on the good wetting of the applied indium to the steel to keep the air from contacting the fresh crack surface. However, we know that in a few tests this did not work. Occasionally we found that a growing crack would slow and stop. A typical potential drop curve in one such test is shown in Figure 11. In such cases, examination under a microscope revealed that the crack had opened to the atmosphere, that is, broken through the indium, as shown in Figure 12. Propagation data from such tests were discarded; it seems possible, however, that even in our successful tests, some gas may have leaked through the apparently unbroken indium coating over the crack and slowed the crack growth somewhat*.

*Additional experiments are being carried out in vacuum.

(b) The propagation times in SMIE are virtually independent of the initial stress applied in the tests (Figures 9 and 10). This argues in favor of a surface diffusion transport mechanism for there is no reason to expect the rate of movement of surface atoms on a crack surface to be influenced by the stress level at the crack tip or within the bulk sample.

(c) The propagation times in SMIE decrease slowly with increasing temperature. The line drawn through the data in Figure 9 was drawn both to best represent the data and to fit Gjostein's (21) ideas for surface self-diffusion on solid metals. In these ideas, at temperatures below about .8 to .9T_{mp}, the surface self-diffusion data should fit an Arrhenius type equation

$$D = D_o \exp\left(-\frac{54\,T_{mp}}{RT}\right) \qquad (2)$$

where the activation energy 54 T_{mp} is given in joules per mole when T_{mp} is in degrees Kelvin; somewhere above .8 to .9T_{mp}, the D values should rise at an increasing rate with temperature up to the melting point. The straight-line portion of the curve in Figure 9 through the data was given a slop of -54 T_{mp} (-23,100 joules/mole or -5600 cals/mole for indium); both the fit here and the higher temperature curvature of the line support the idea that indium self-diffusion is the controlling transport mechanism in SMIE.

Crack Initiation

The meaning of the time, t_i, which we have defined as the crack initiation time, needs some clarification. Strictly, this is the time at which the crack first reaches a size – about .15 mm^2 in area – detectable by our potential drop measurements. However, the interrupted delayed failure tests showed that any crack existing at .9 t_i could be no larger than about 10^{-4} times the size at t_i, whereas in SMIE at 1.1 t_i the potential drop curves (Figures 7 and 8) show that the crack size is no more than about 3-4 times that at t_i. Thus, in SMIE, there is clearly a drastic decrease in crack growth rate between .9 t_i and t_i. We interpret this to mean that at this point there is a change in the rate-controlling mechanism of crack formation – from control by some crack initiating process to control by the embrittler transport process. This is illustrated schematically in the upper diagram of Figure 13. Here, the time for the crack initiating process (line df) and for embrittler transport from source to crack

tip (line ae) are plotted versus crack size. At crack sizes below the point of intersection, b, of these two lines, the time for transport is much shorter than that for the crack initiation process, so the latter gives the crack formation time; beyond point b, the opposite is true. As a result, the crack formation time is given by the path d b c in the figure. In LMIE, the situation is as indicated schematically in the lower diagram of Figure 13. Here, the embrittler transport time (line ac) is very short throughout crack formation; therefore, the initiation process controls crack formation at all times, leading to the growth path d b f. In both SMIE and LMIE, then, t_i is a measure of the point b. We know that at earlier times, the curve drops precipitously to below point e, the point delineated by the delayed failure tests; the shape of the curve at nucleation of the crack is not known. We have made the assumption, however, that whatever its shape, this is constant from sample to sample, and have, thus, taken t_i as a measure of the initiation process kinetics. The discussion of crack initiation below and in Part II of this presentation is based on this assumption.

The experimentally determined crack initiation times at two different levels are plotted versus temperature for both SMIE and LMIE in Figure 14. Again, within the experimental scatter a number of clear characteristics can be seen:

(a) The data for both stress levels and for both SMIE and LMIE can be represented by Arrhenius type equations. This suggests strongly that the underlying process involved during the crack-incubation period is thermally activated. Further, since the slopes of all the straight lines through the data are the same within experimental error, the process is indicated to be basically the same for both LMIE and SMIE, and for the different stress levels. From the slopes, the average apparent activation energy* of this process is 155 ± 3-1/2 kjoules/mole (37.0 ± 0.8 kcals/mole).‡

(b) Since the lines in Figure 14 are displaced upward on decrease in stress, it is clear that the rate of the underlying process is stress dependent, increasing with increasing stress.

---

*The activation energy is "apparent" because, as described in Part II of this presentation, we believe it is actually the sum of two activation energies.

‡The experimental errors given in this paper for activation energies are actually reproducibilities based on the three lines in Figure 13. For one standard deviation, the errors of the activation energies, based on the variance in regression analysis, average to ± 19 kjoules/mole (± 4.5 kcals/mol).

(c) At the melting point, the initiation time increases discontinuously by a factor of about 6.5 in going from LMIE to SMIE, though the slopes of the corresponding lines do not differ. To confirm the presence of this gap, a series of tests was run at several other stress levels at the two temperatures 154°C (just below the indium melting point) and 158°C (just above the indium melting point); the results are given in Figure 15. It may be seen that the ratio of initiation times across the gap at the melting point persists unchanged, within a substantial scatter, for all stress levels at which delayed failure takes place, that is, down to 1068 MPa (155 ksi). Below this stress level, no failure took place at all – at least within the patience of the experimenters (to times of about 11 days). Thus, there is a "threshold" stress level – as found in most previous MIE studies – below which MIE delayed failure does not take place. In the present case, the threshold stress is just above the macroscopic proportional limit of 1040 MPa (151 ksi). Above the threshold stress, the initiation times decrease approximately linearly with increasing stress both in SMIE and LMIE.

Theoretical aspects of crack initiation based on the above results and the general literature are described in Part II of this presentation, which follows directly.

CONCLUSIONS

In the fracture of 4140 steel due to MIE by indium:

(1) Crack initiation and crack propagation are separate stages in crack formation, each being thermally activated with quite different activation energies.

(2) In LMIE, crack propagation is extremely rapid, taking place in less than .1 second (for crack depths of the order of 1-2 mm).

(3) Theory and the experimental results indicate embrittler transport to the crack tip in LMIE is by bulk liquid flow.

(4) In SMIE, crack propagation is much slower (500-2000 seconds for a depth of .7 mm); it is controlled by embrittler transport which takes place by indium surface self-diffusion.

(5) Crack initiation in both LMIE and SMIE exhibits an incubation period; at constant stress the initiation time increases with decreasing temperature according to an Arrhenius-type relation; it also increases with decreasing stress.

(6) The apparent activation energy for crack initiation time is the same, within experimental error, in LMIE and SMIE, having a value of $155 \pm 3\text{-}1/2$ kj/mole ($37 \pm .8$ kcals/mole). This apparent activation energy showed no change on raising the applied stress from 1158 to 1226 MPa (168 to 178 ksi).

(7) At constant stress, the initiation time at the melting point of indium is larger by a factor of 6.5 in SMIE than in LMIE. This time gap at the melting point persists at about the same value over the stress range tested – from 1068 to 1226 MPa (155 to 178 ksi).

REFERENCES

1. J. C. Lynn, W. R. Warke, and Paul Gordon: Mater. Sci. Eng., 1975, Vol. 18, pp. 51-62.
2. N. S. Stoloff and T. L. Johnston: Acta Met., 1963, Vol. 11, pp. 251-56.
3. A. R. C. Westwood and M. H. Kamdar: Phil. Mag., 1963, Vol. 8, pp. 787-804.
4. W. M. Robertson: Trans. TMS-AIME, 1966, Vol. 236, pp. 1478-82.
5. E. E. Glikman, Y. V. Goryunov, V. M. Demin, and K. Y. Sarycher: Izvest. Vyss. Ueheb. Zav. Fizika, 1976, May, No. 5, pp. 7-15, 15-23; ibid July 1976, pp. 17-22, pp. 22-29.
6. M. A. Krishtal: Sov. Phys. Dokl. 1970, Vol. 15, No. 6, pp. 614-17.
7. S. P. Lynch: ARL Mat. Reports No. 101, 102, Dept. of Defense, Melbourne, Victoria, Australia, 1977.
8. W. Rostoker, J. M. McCaughey, and H. Markus, Embrittlement of Liquid Metals, Reinhold Publ. Co., N. Y., 1960.
9. L. S. Bryukhanova, I. A. Andreeva, and V. I. Likhtman: Sov. Phys.-Solid State, 1962, Vol.3, pp. 2025-28.
10. H. Nichols and W. Rostoker: Trans. ASM, 1965, Vol. 58, pp. 155-163.
11. Y. Iwata, Y. Asayama, and A. Sakamoto: Nippon Kinzaku Gakkaishi (J. Japan Inst. Met.), 1967, Vol. 31, pp. 77-83.
12. J. V. Rinnovatore, J. D. Corrie and H. Markus: Trans ASM, 1966, Vol. 59, pp. 665-671.
13. C. M. Preece and A. R. C. Westwood: Fracture, 1969, Proc. Sec. Intl. Conf. on Fracture, pp. 439-450.
14. J. Zych: M. S. Thesis, Illinois Institute of Technology, 1977.
15. J. C. Lynn: Ph. D. Thesis, Illinois Institute of Technology, 1974.
16. M. E. Kassner: M. S. Thesis, Illinois Institute of Technology, 1977.
17. F. N. Rhines, J. A. Alexander and W. F. Barclay: Trans ASM, 1962, Vol. 55, pp. 22-44.
18. Paul Gordon: Met. Trans. A., 1978, Vol. 9A, pp. 267-273.
19. B. D. Summ, P. A. Rutman, Y. V. Goryunov: Fiziko-Khim. Mekban. Mater., 1973, Vol. 9, pp. 50-53.
20. P. Shewmon: Diffusion in Solids, McGraw-Hill, N. Y., 1963.
21. N. A. Gjostein: Diffusion, ASM, Metals Park, Ohio, 1973, pp. 241-74.

ACKNOWLEDGEMENTS

We are indebted to the National Science Foundation for financial support of this research from its inception under contracts DMR 7704272 and DMR 7908674, and to the Office of Naval Research for financial support during its last year under contract No. 0014-79-C0580.

We also appreciate the assistance of Alan Druschitz, a Ph. D. candidate in the Dept. of Metallurgical and Materials Engineering, Illinois Institute of Technology, for supplying the fractographs of Figure 4, and for carrying out the hydrogen embrittlement tests referred to in the description of experimental details.

In addition, thanks are due to M. E. Kassner who did a considerable amount of the preliminary work which helped lay the groundwork for the research reported here.

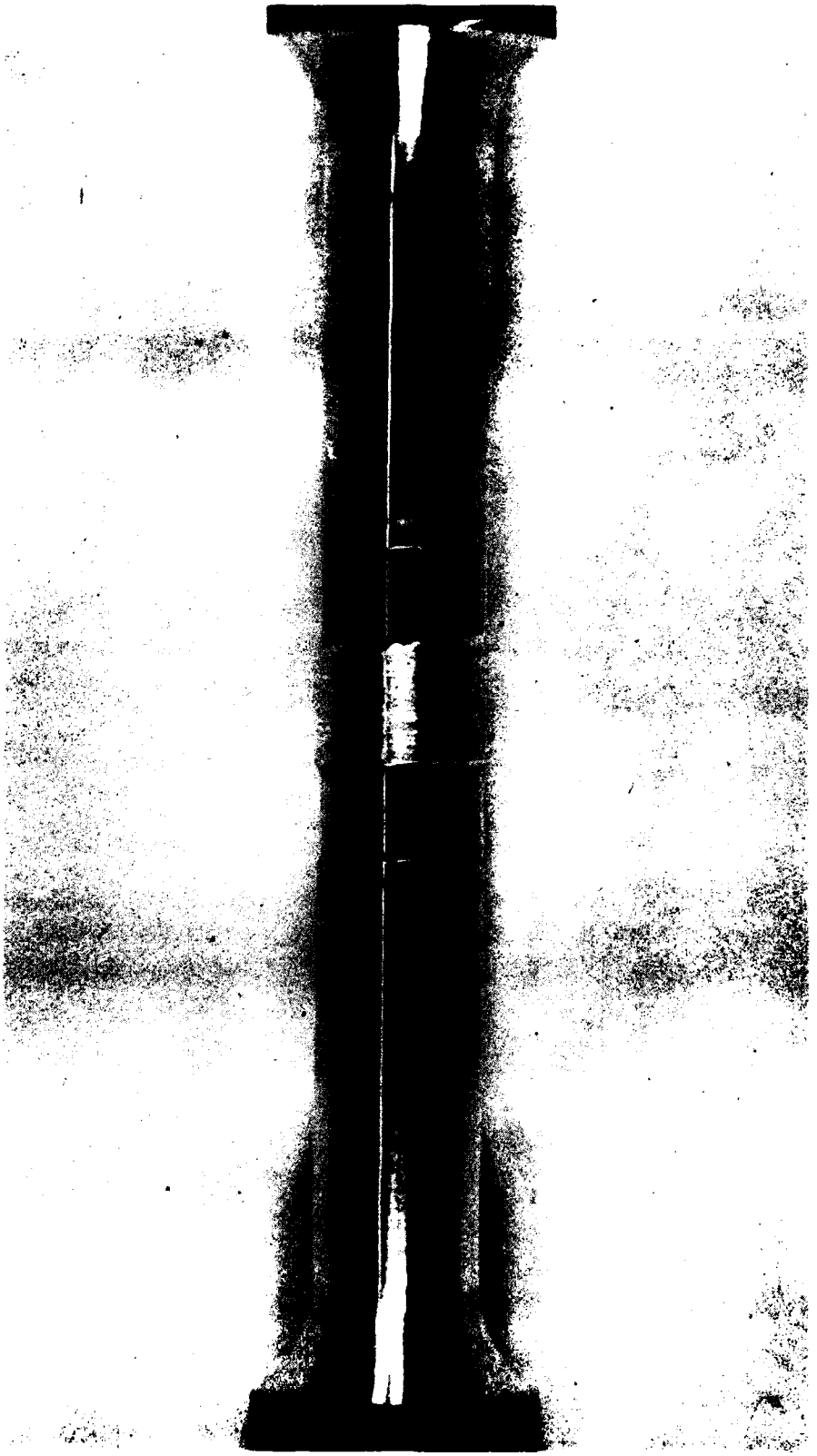

Figure 1. Typical specimen, with indium applied. Approx. 4X

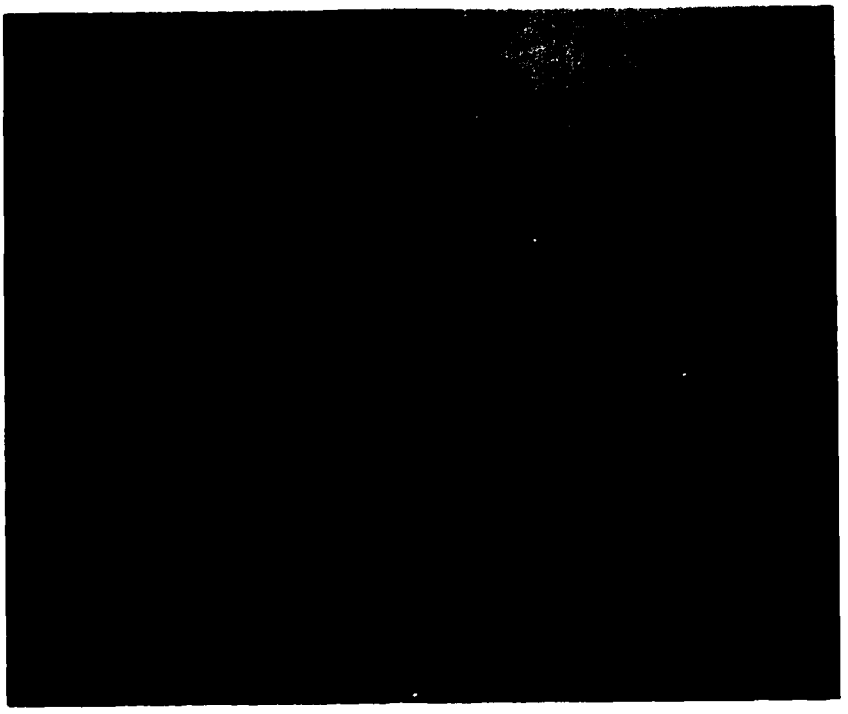

a

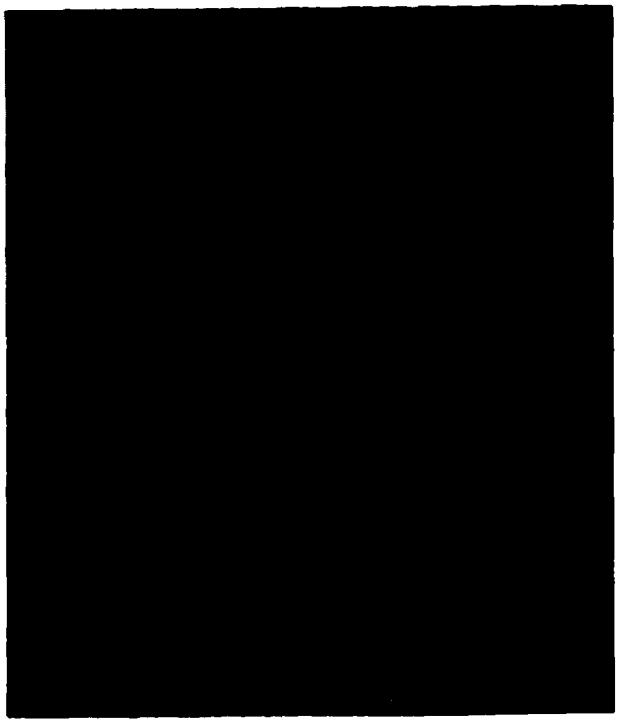

b

Figure 2. Deep-etched surface of sample after interrupted delayed failure test. Longitudinal lines (vertical) are inclusion markings.
(a) 22X, showing full width of sample (horizontal);
(b) 150X

Figure 3. Typical fracture surface, SMIE. Approx. 11X

a

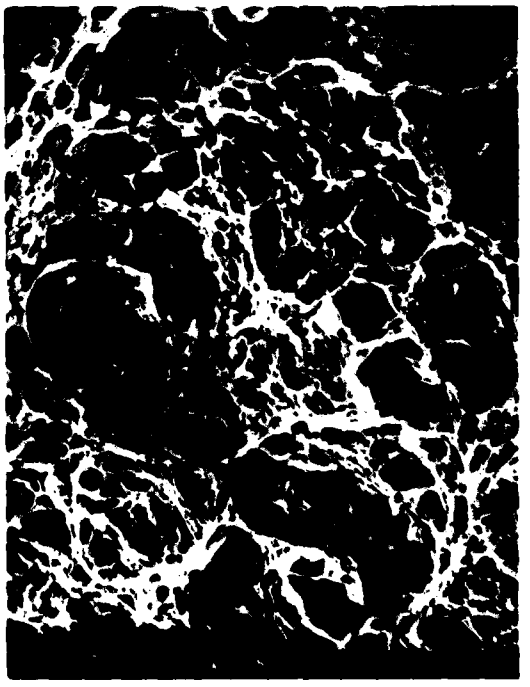

b c

Figure 4. SEM fractographs in (a) embrittler-controlled portion of SMIE fracture, 1100X; (b) ductile portion of fracture, 1600X; (c) at brittle-to-ductile change-over, 1600X

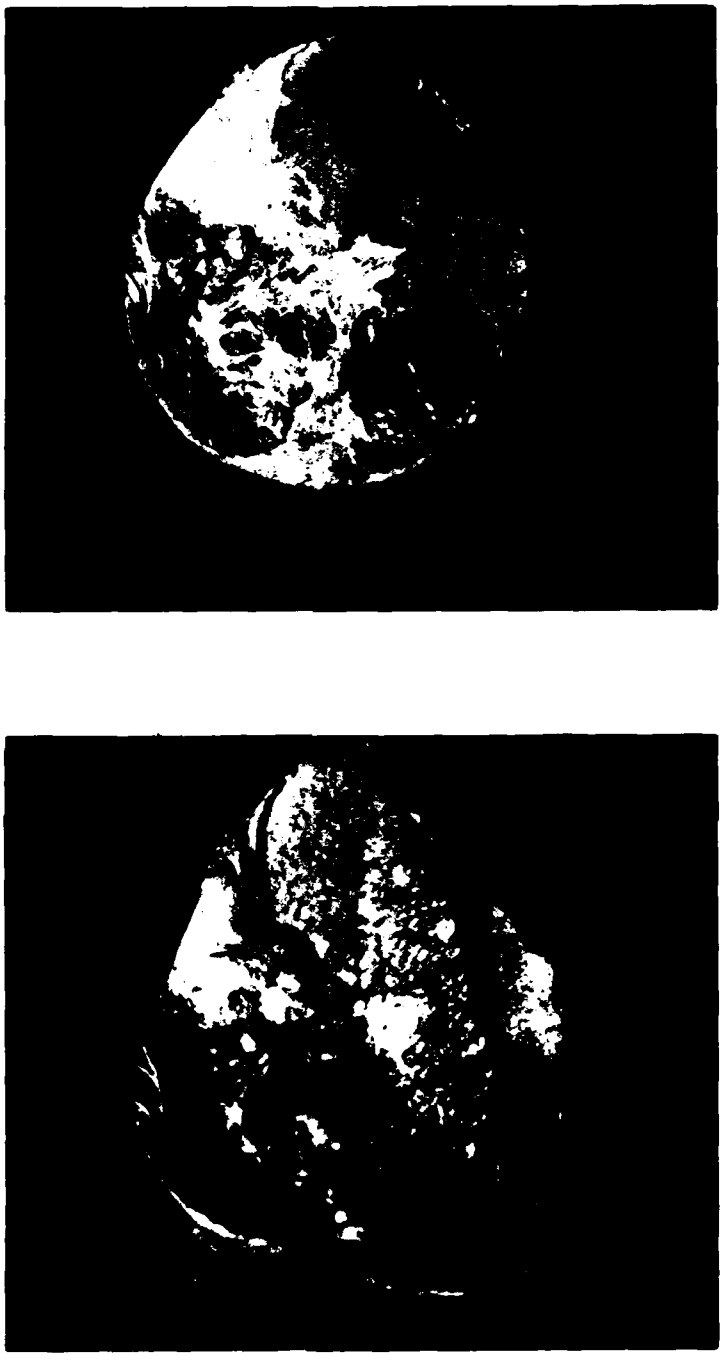

Figure 5. Typical fracture surface, LMIE. Approx. 11X

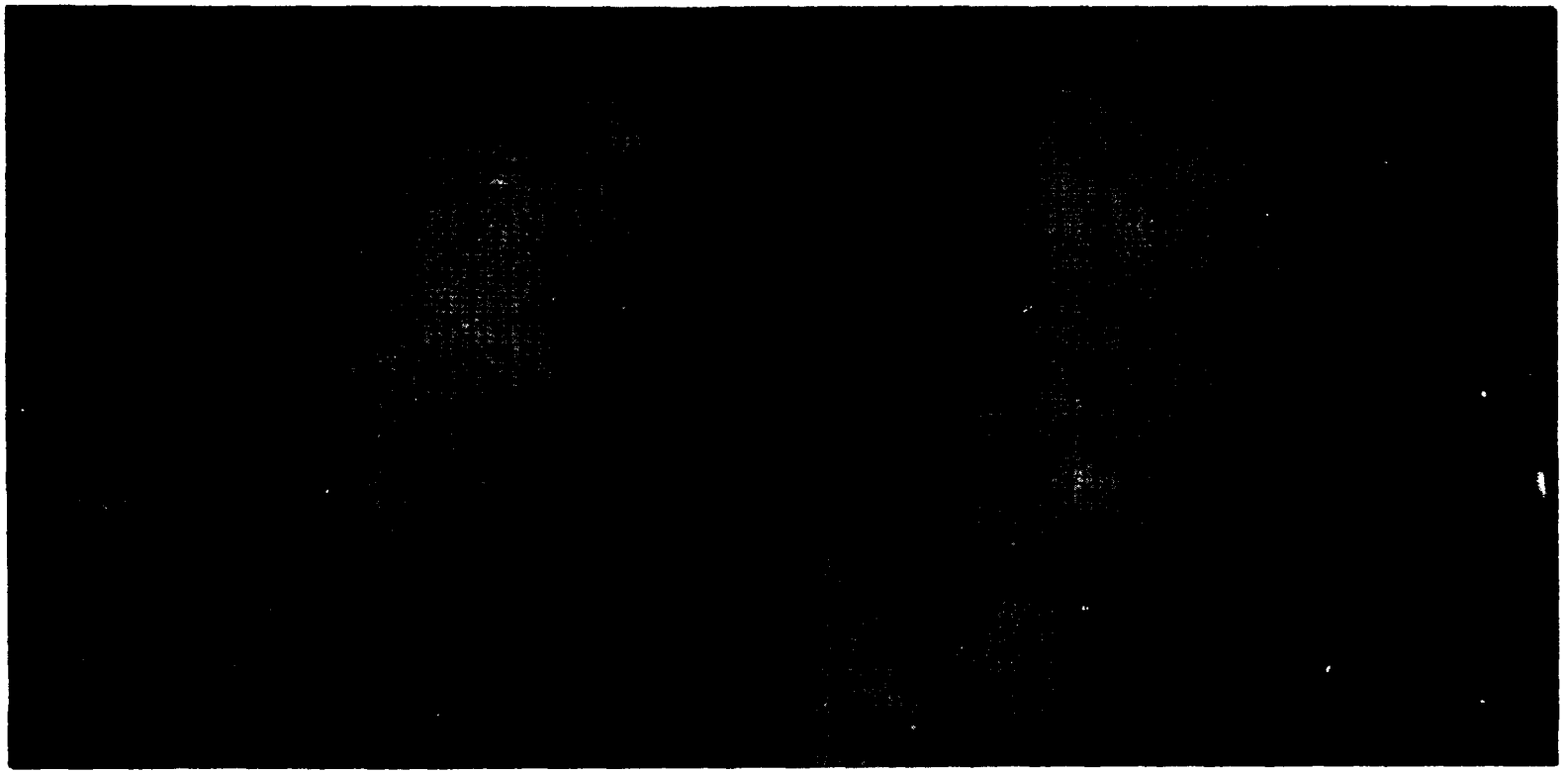

Figure 6. Typical potential drop-time curve in LMIE

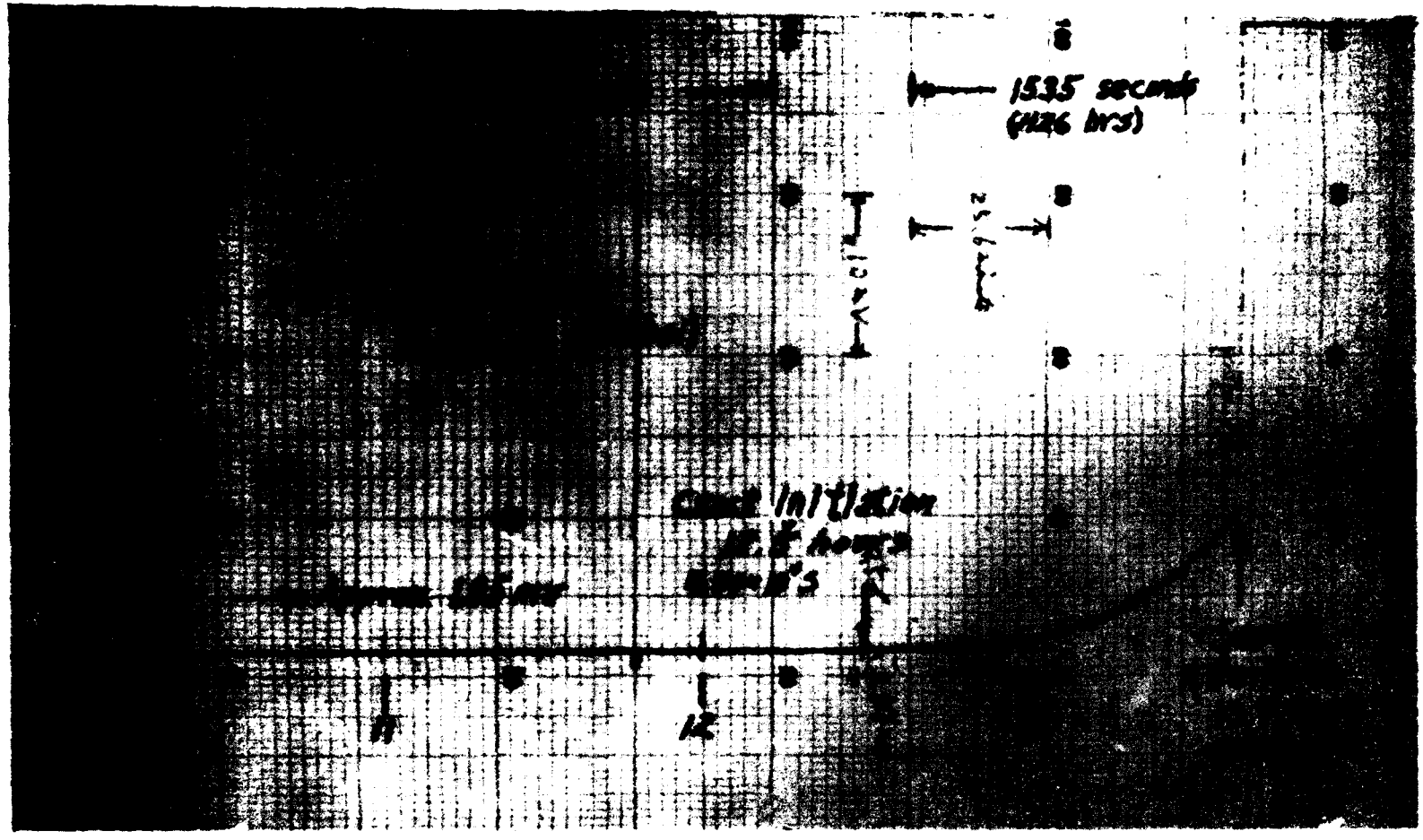

Figure 7. Typical potential drop-time curve in SMIE

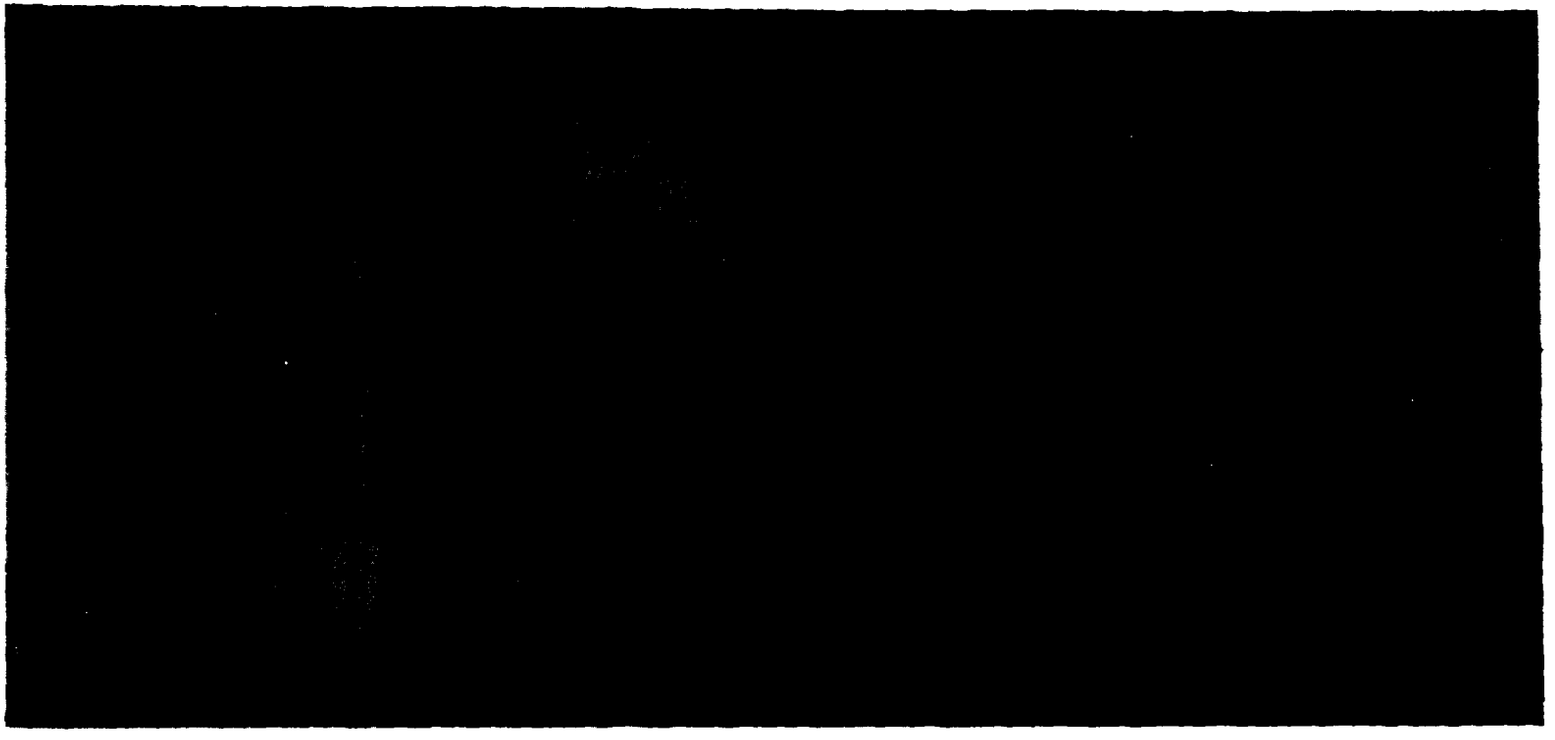

Figure 8. Typical potential drop-time curve in SMIE

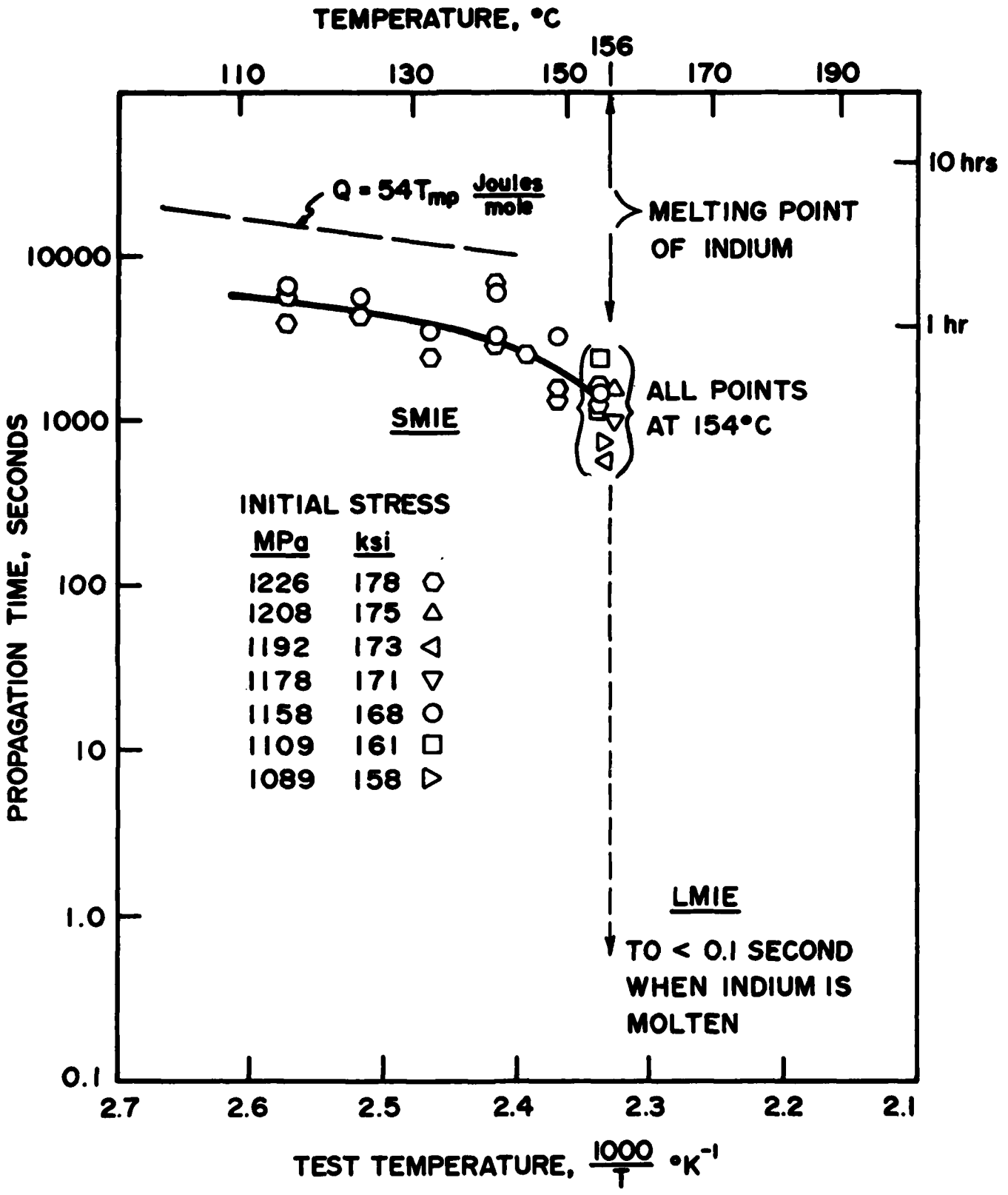

Figure 9. Propagation time vs temperature at various initial stress levels

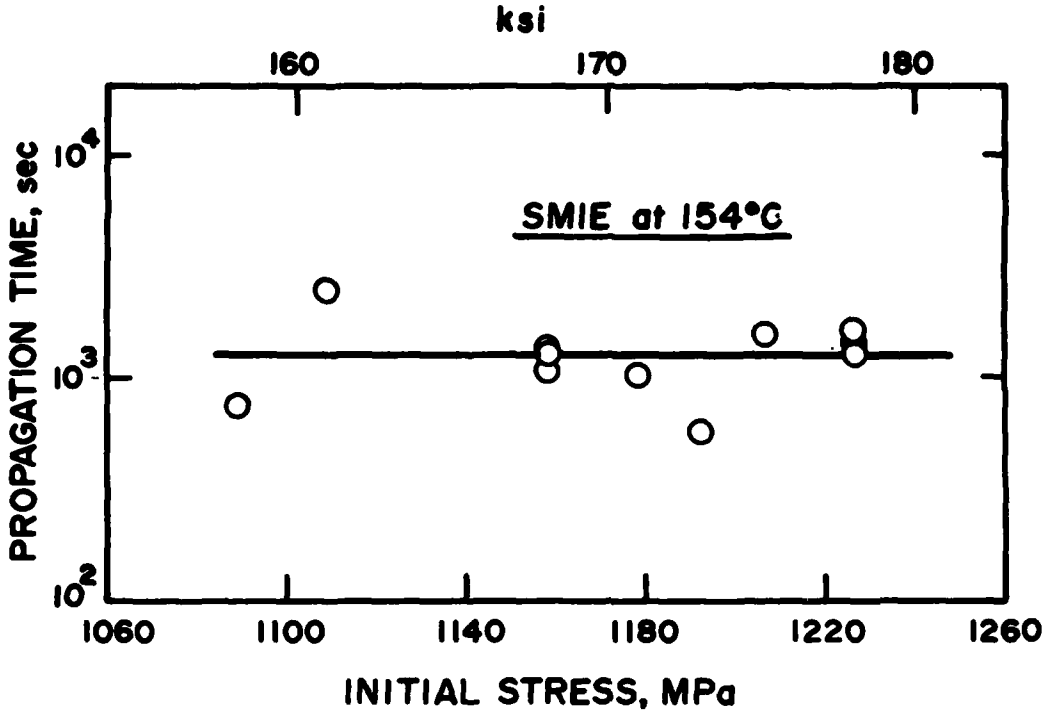

Figure 10. Propagation time vs initial stress in SMIE at 154°C

Figure 11. Typical potential drop-time curve in SMIE for sample in which crack formed and stopped growing

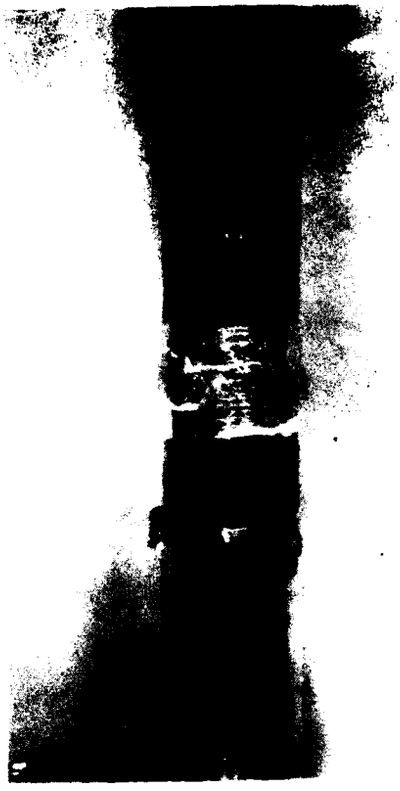

a

b

Figure 12. Crack broken through indium coating on sample in which crack formed and stopped growing.
(a) Approx. 3X
(b) 150X

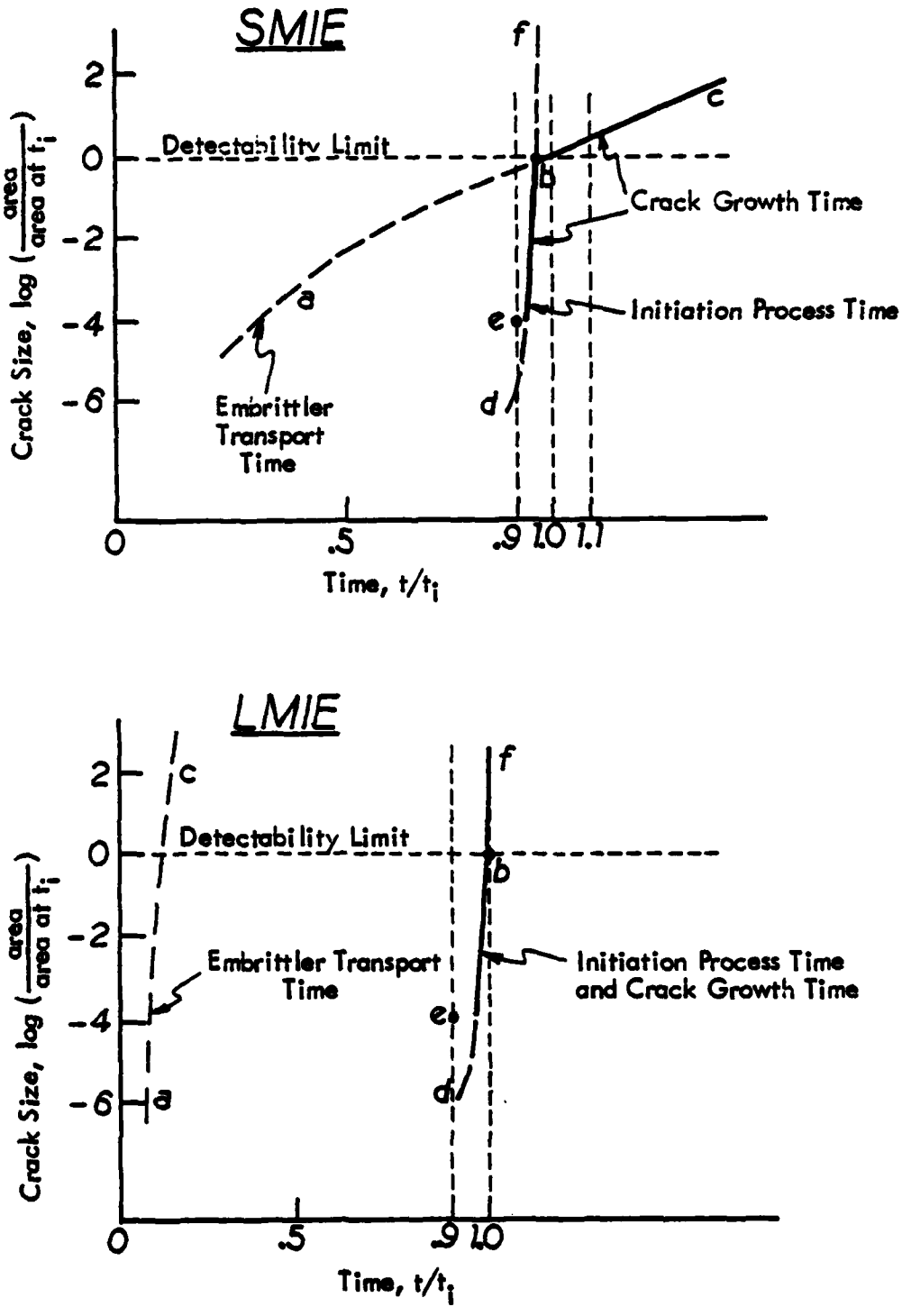

Figure 13. Schematic representation of crack growth paths in SMIE and LMIE

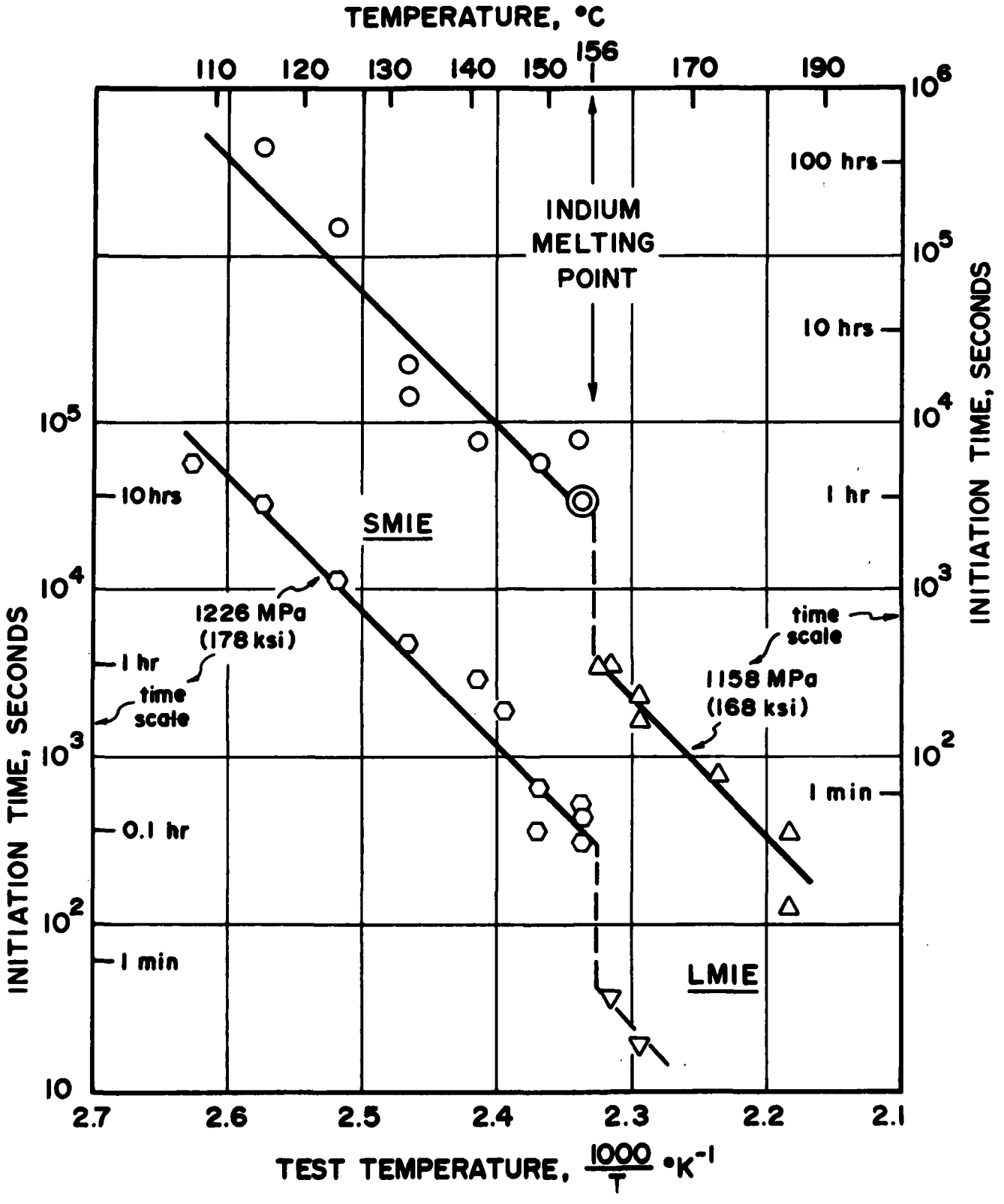

Figure 14. Initiation time vs temperature in SMIE and LMIE at two stress levels

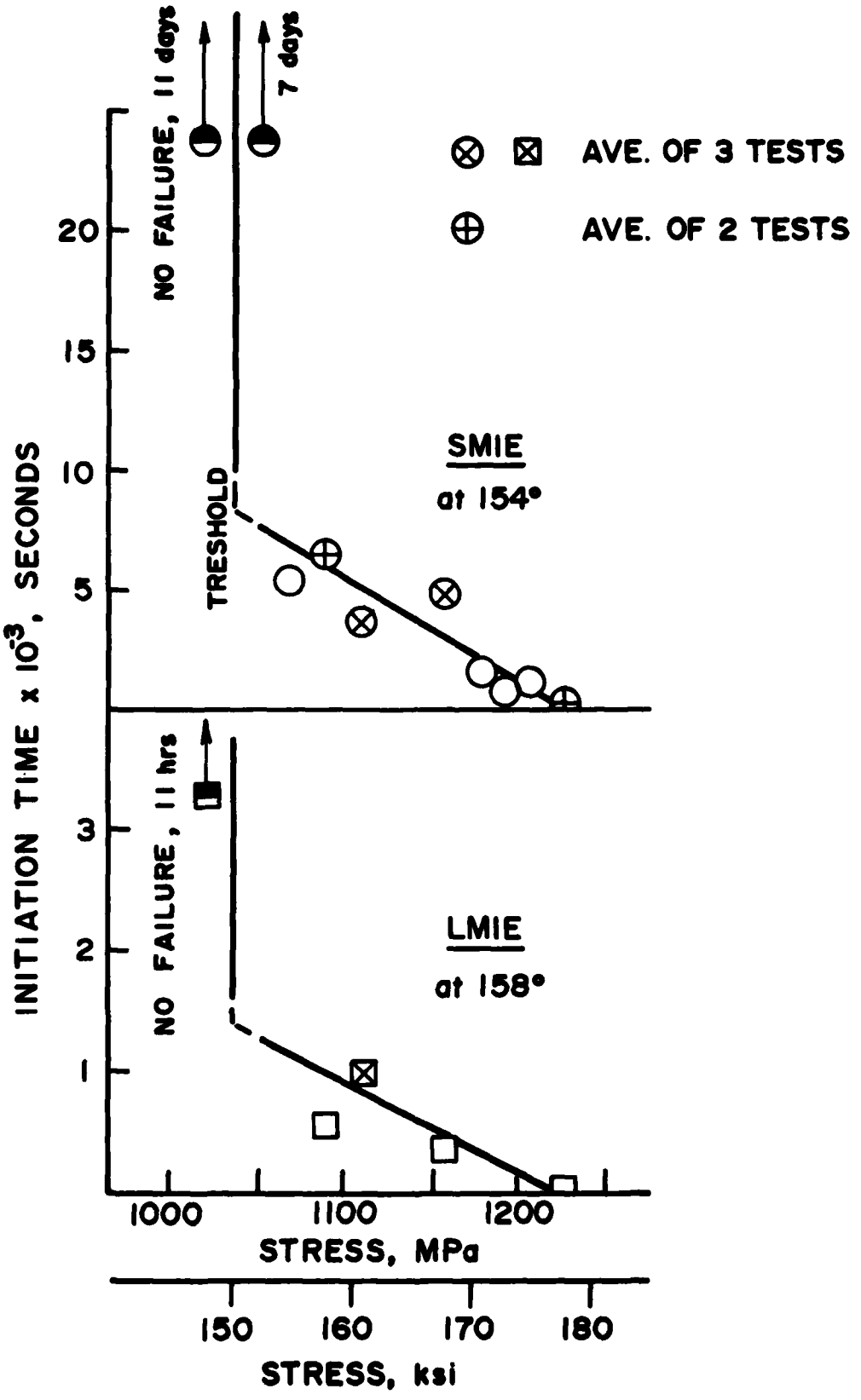

Figure 15. Initiation time vs stress level in SMIE and LMIE near indium melting temperature


DATE
ILME